


Article

Optimization of Geopolymers for Sustainable Management of Mine Tailings: Impact on Mechanical, Microstructural, and Toxicological Properties

Gregorio Palma ^{1,*}, Héctor Bolaños ², Roberto Huamani ², Cara Clements ³  and Ahmadreza Hedayat ³ 

¹ Escuela profesional de Ingeniería Química, Facultad de Ingeniería de Procesos, Universidad Nacional de San Agustín (UNSA), Arequipa 04000, Peru

² Escuela profesional de Ingeniería Metalúrgica, Facultad de Ingeniería de Procesos, Universidad Nacional de San Agustín (UNSA), Arequipa 04000, Peru; hbolanos@unsa.edu.pe (H.B.); rhuamanibe@unsa.edu.pe (R.H.)

³ Department of Civil and Environmental Engineering, Colorado School of Mines, 1500 Illinois St., Golden, CO 80401, USA; caraclements@mines.edu (C.C.); hedayat@mines.edu (A.H.)

* Correspondence: gpalma@unsa.edu.pe

Abstract: This study investigates the use of geopolymer technology as an alternative for the management of mine tailings, which is a serious environmental problem in mining areas, including the Arequipa region of Peru. In this study, the mixture of stabilized mine tailings with different percentages of binders (i.e., metakaolin and pumice) and their impact on the mechanical, microstructural, and toxicological properties of the synthesized geopolymers were analyzed. The ratios of mine tailings to binder material varied between 100/0 and 0/100. The activation was carried out with an alkaline solution of sodium hydroxide (10 M) and sodium silicate (modulus 2.5). Specimens were fabricated as 50 mm cubes, and the seven mix designs were evaluated in triplicate. The evaluations included compressive strength at 7, 14, 28, and 56 days of curing, chemical analysis by Fourier Transform Infrared Spectroscopy (FT-IR), microstructural characterization by X-ray diffraction (XRD) and Scanning Electron Microscopy (SEM/EDS), thermal behavior by thermogravimetry and differential thermal analysis (TGA/DTA) between 40 °C and 1000 °C, and toxicological tests by the Toxicity Characteristic Leaching Procedure (TCLP, EPA 1311) to determine the efficiency of immobilization of toxic metals. The results demonstrate significant improvements in compressive strength for the F50 specimens compared to A0, with increases of approximately 300%, 270%, and 461% observed at 7, 28, and 56 days of curing, respectively, with microstructural stability with an average pore size of 7.21 μm, and efficiency in the immobilization of heavy metals in geopolymers with 30% or 40% binder (60%–70% mine tailings). The leachate concentrations of As, Cd, Pb, and Hg were below the established thresholds, indicating that the stabilized mine tailings can be classified as “non-hazardous materials”. Geopolymers with 30% to 50% binder showed strength development with microstructural stability and efficiency in the immobilization of heavy metals, complying with current regulations. Therefore, these geopolymers are suitable for various applications and in different environmental conditions.

Keywords: mine tailings; geopolymer; stabilization of heavy metals; encapsulation of heavy metals; metakaolin; pumice; compressive strength



Citation: Palma, G.; Bolaños, H.; Huamani, R.; Clements, C.; Hedayat, A. Optimization of Geopolymers for Sustainable Management of Mine Tailings: Impact on Mechanical, Microstructural, and Toxicological Properties. *Minerals* **2024**, *14*, 997. <https://doi.org/10.3390/min14100997>

Academic Editors: Dariusz Mierzwiński and Wei-Ting Lin

Received: 6 August 2024

Revised: 10 September 2024

Accepted: 22 September 2024

Published: 30 September 2024



Copyright: © 2024 by the authors. Licensee MDPI, Basel, Switzerland. This article is an open access article distributed under the terms and conditions of the Creative Commons Attribution (CC BY) license (<https://creativecommons.org/licenses/by/4.0/>).

1. Introduction

Mine tailings (MTs) are byproducts of mineral extraction that contain potentially toxic heavy metals (PTHMs) such as arsenic (As), cadmium (Cd), mercury (Hg), lead (Pb), and zinc (Zn) [1]. Those PTHMs and other residual chemical compounds from mineral processing [2] make MTs a source of contamination and a serious environmental threat that requires improved management techniques.

MTs require vast expanses of land for storage, emit particulate matter in the surrounding urban and agricultural areas, and cause long-term accumulation of mining environmental liabilities (PAM). Additionally, tailings with high concentrations of heavy metals can generate acid mine drainage due to climatic conditions such as precipitation.

To reduce potential environmental impacts, there are three possible technological approaches: (1) isolation of MT, (2) chemical stabilization of MT, and (3) a combination of both [3]. Among these methods, geopolymerization offers an environmentally safe technology to stabilize and encapsulate the PTHMs present in MT within the geopolymer matrix [4,5].

Geopolymers are compounds derived from aluminosilicate raw materials that are activated by reaction with a highly alkaline solution, resulting in a three-dimensional structure similar to organic polymers [6,7]. The most common activators are sodium or potassium hydroxide, silicates, and carbonates [8].

When MTs are used to prepare geopolymers, the high silica content increases the $\text{SiO}_2/\text{Al}_2\text{O}_3$ molar ratio, which can negatively affect the geopolymerization reactions. To solve this problem, metakaolin (MK) is used as an additional source of aluminum (Al) due to its high reactivity, homogeneity, and purity [9].

Additionally, using MTs as the sole precursor generally leads to lower compressive strength, so it is considered feasible to improve it by incorporating supplementary material [10].

Geopolymerization technology has successfully been used to produce geopolymer concrete. Geopolymer concrete uses silica-alumina-rich materials instead of cement. Youssf et al. [11] evaluated the performance of geopolymer concrete by replacing sand with lightweight materials such as rubber, vermiculite, and lightweight expanded clay aggregate (LECA) in different proportions. LECA improved compressive strength but negatively affected shear strength in concrete slabs. Geopolymer concrete with 60% LECA was suitable for structures subjected to axial loads. The use of construction and demolition (C&D) waste in geopolymer concrete has also been reported successfully. Elemam et al. [12] partially replaced granulated blast furnace slag (GGBFS) and fine aggregate with brick dust (CBP) and fine clay brick (FCB) to produce high-strength geopolymer concrete. The optimal mixtures included 5% CBP, 5% fly ash (FA), and 40% FCB, achieving acceptable mechanical properties and better resistance to carbonation and freezing. Khattab et al. [13] demonstrated that by using magnetized water instead of tap water to prepare an alkaline activator in FA-based geopolymer concrete, a significant improvement in its properties was achieved. In particular, using magnetized water increased the workability of concrete by up to 100% and the compressive strength by 193%, 192%, and 124% at 7, 28, and 56 days, respectively, compared with tap water. These results suggest that magnetized water alkali activator-prepared geopolymer concrete could represent a new class of green concrete with promising structural applications.

Previous research has produced geopolymers using gold MTs, ground granulated blast furnace slag (GGBFS), and MK in proportions of 40%–50%, 20%–30%, and 30%, respectively. The effectiveness of immobilization was evaluated through leaching tests after 7 and 28 days of curing and again after 18 months. Specimens were immersed in water for one day, and the metallic leachates in the solution were determined by ICP-OES. Several elements, such as Cr, Cu, Ni, Zn, and Mn, were almost completely immobilized, and the immobilization efficiency improved with a longer curing time [14].

In a study on the effectiveness of solidification/stabilization of zinc mine tailings through geopolymerization, geopolymers were made from MK and MTs. Specimens synthesized without MK had a strength of 1.1 MPa, but when the MK content was increased to 50%, the mechanical strength increased to 30.1 MPa. In the SEM images of the 50% MK geopolymer, the gel reaction products were sufficient to encapsulate the unreacted crystals. The presence of andradite and more crystalline quartz in the MTs was suggested to reduce the amount of gel produced during geopolymerization. The results of the TCLP tests showed that the Zn concentration increased from 12.7 to 58.2 ppm as the MK amount decreased, while for the

50% MK specimen, the Zn concentration was 2.7 ppm, and the percentage of Zn leached was 0.91% of the total Zn in the tailings, demonstrating that Zn was immobilized [15].

Pumice (PP) is a material composed mainly of SiO₂ and Al₂O₃ [16], making it suitable for the manufacture of geopolymers. The geopolymers made from PP achieved the highest compressive strength of 40 MPa with the optimal mix design parameters: silica modulus Ms = 0.68, Na₂O = 0.10%, and water/binder ratio = 0.36 [17].

However, there is limited research on the use of pumice as a raw material in the production of mine tailing-based geopolymers or in a blended system with MK or fly ash [4,5,9]. Therefore, pumice should be investigated and explored as another potential resource for producing geopolymers that can help in the stabilization and encapsulation of heavy metals.

The objective of this study is to evaluate the mechanical, toxicological, and microstructural behavior of geopolymers made from MTs, MK, and PP by varying the MTs content in their composition from 100% to 0% of the total solids, including the MK, PP, and MTs. The aim is to obtain a specimen that contains the highest possible amount of MTs while ensuring optimal mechanical, toxicological, and microstructural properties for its long-term integrity and durability. Possible applications of the produced geopolymers include safety fills or alternative construction materials.

2. Materials and Methods

2.1. Materials

The materials utilized in this study included the following: MTs [18]; MK and PP as binder materials; and sodium hydroxide and sodium silicate solution as alkaline activators. Additional materials employed included a commercial superplasticizer admixture and distilled water.

2.1.1. Mining Tailings (MTs)

Tailings samples were obtained from the mineral processing plant of the mining company Paraíso, located in Chala district, province of Caraveli, Arequipa region, Peru. Sample collection was conducted following the Soil Sampling Guide from the Ministry of Environment (MINAM-2014), ensuring the representativeness of the sample within the sampling area.

Out of all the various MTs analyzed from around the Arequipa region, the ones from the Paraíso Mining Company were some of the most contaminated. The elemental composition of different MT sources is shown in Tables 1 and 2, and the mineralogical composition is shown in Table 3. Concentrations of heavy and toxic metals (HTM) were determined using the multi-element assay method by ICP-OES with acid digestion, utilizing the PerkinElmer AVIO-550 max instrument. Analysis of the particle size distribution of the Paraíso tailings showed a D₉₀ of 65 µm, signifying that 90% of the particles were smaller than a 65 µm screen size.

Table 1. Chemical composition expressed as total metals (mg/kg) of the mining environmental passive samples from the Arequipa region.

Samples of Mining Environmental Liabilities	Toxic Heavy Metals				
	Arsenic (As)	Cadmium (Cd)	Lead (Pb)	Mercury (Hg)	Zinc (Zn)
Kiowa-Au	49.9	1.47	168.22	0.1	21
Kiowa-Cu	291.9	2.42	1585.8	0.2	161.9
Topacio	609.6	29.75	828.72	8.1	1221
Coriminas	145	4.17	191.47	0.6	205.2
Madrigal	195	6.03	2290.49	0.4	323.3
Secocha	160.1	21.95	1028.8	276	375.3
Century	28	2.25	21.27	0.1	21.1
Mollehuaca	2052.2	7.96	875.74	193.1	41.3
Paraíso	6001	332.54	2081.87	35	2309
Otapara	26.3	9.29	12.71	0.8	23.4

Table 2. Toxicological analysis of samples (mg/L) of mining environmental liabilities from the Arequipa region.

Samples of Mining Environmental Liabilities	Toxic Heavy Metals				
	Arsenic (As)	Cadmium (Cd)	Lead (Pb)	Mercury (Hg)	Zinc (Zn)
Kiowa-Au	0.011	<0.004	0.237	<0.003	0.051
Kiowa-Cu	0.023	0.063	0.01	<0.003	9.286
Topacio	0.587	0.201	0.034	0.003	2.612
Coriminas	0.051	0.005	<0.005	<0.003	0.317
Madrigal	<0.006	0.072	0.020	<0.003	6.162
Secocha	<0.006	0.005	0.403	0.026	0.139
Century	<0.006	<0.004	0.008	<0.003	0.093
Mollehuaca	0.020	0.004	0.071	<0.003	0.071
Paraíso	0.393	0.046	0.590	0.041	1.828
Otapara	<0.006	<0.004	0.006	<0.003	0.105

Figure 1 shows the SEM micrograph and EDS analysis of the MTs, whereas Figure 1e depicts the morphology of the tailings as particulate grains stacked freely without segmentation, exhibiting various angular and irregular geometries of varied sizes. No predominant angular shape is observed, consistent with other analyses [19].

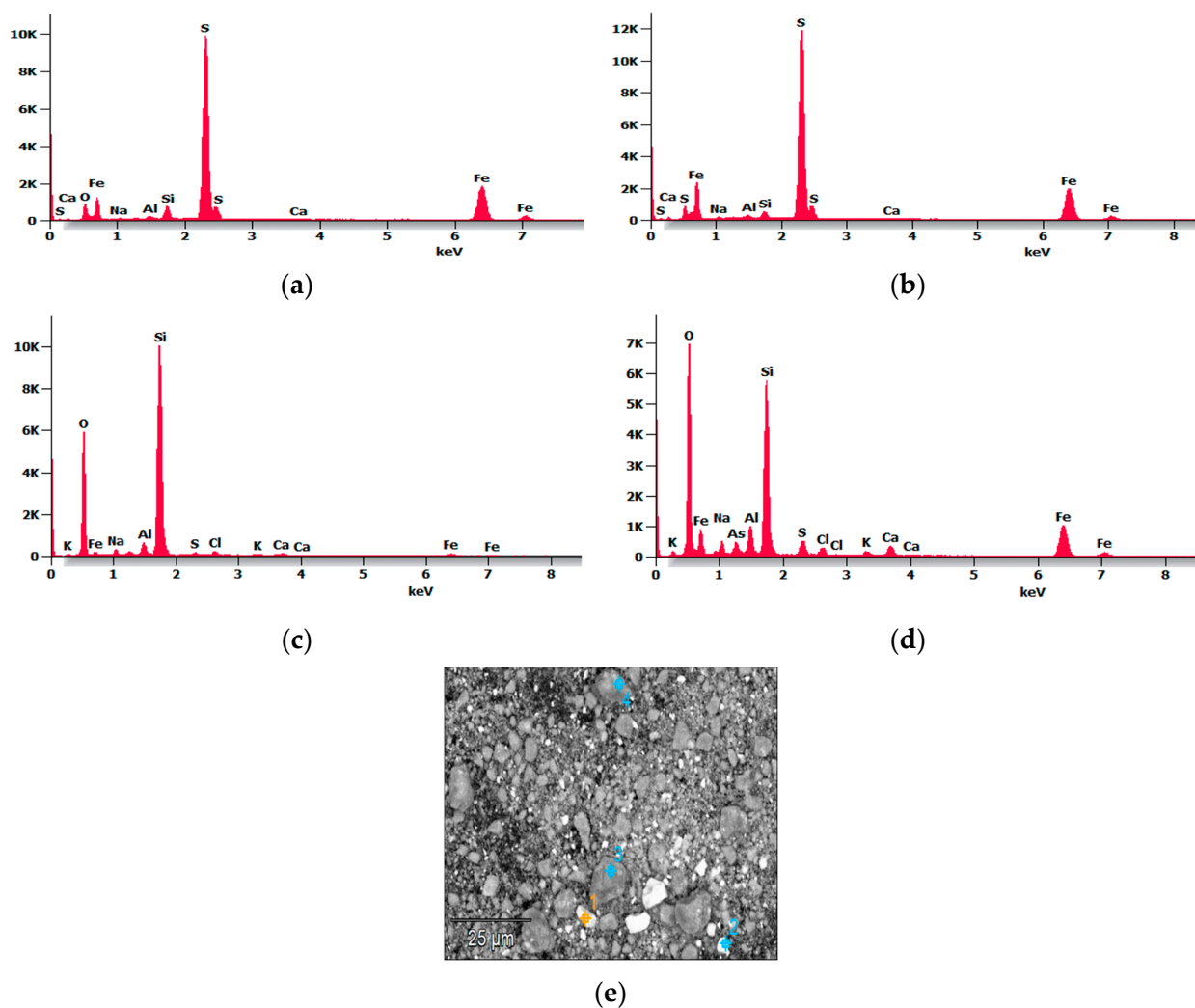


Figure 1. Microstructural analysis of MTs: EDS with four-point samples at (a) point 1, (b) point 2, (c) point 3, and (d) point 4, and (e) Scanning Electron Micrograph.

Figure 1a–d presents the EDS spectra from the four points identified in the SEM micrograph shown in Figure 1e.

The results indicate that in Figure 1a,b, sulfur shows a peak of higher intensity, and iron appears with moderate intensity, followed by Al, Si, and Ca as main components, while Figure 1c,d shows two peaks of higher intensity corresponding to Si and O₂, followed by Fe, Al, and Ca. It is noteworthy that arsenic (As) and chlorine (Cl) appear in Figure 1d but not in the spectra taken from other MT particles (Figure 1a–c). The intensity of Al in the MTs was quite low, according to Figure 1; therefore, it was necessary to mix tailings with amorphous aluminosilicates such as MK and PP to adjust the Si:Al ratio to enhance reactivity and thereby improve the geopolymerization process.

Table 3. Mineralogical analysis of the sample of the “Paraíso” environmental liability.

Mineral Name	General Formula	% in Weigh
Quartz	SiO ₂ + varied composition	60.7
Pyrite	FeS ₂	15.39
Arsenopyrite	FeAsS	9.30
Chalcopyrite	CuFeS ₂	6.40
Goethite	Fe ³⁺ O(OH)	4.27
Galena	PbS	2.29
rutile	TiO ₂	1.30
Sphalerite	ZnS	Trace
Covellite	CuS	Trace
Pyrrhotite	Fe(1 – X)S	Trace
gray coppers	varied composition	Trace

2.1.2. Pumice (PP)

PP is a volcanic mineral material composed mainly of silica and alumina, approximately 70% SiO₂ and 13% Al₂O₃, as shown in Figure 2b [20]. Before geopolymerization, the PP was sieved through a #200 mesh (88% passing). Then, it underwent thermal treatment in a furnace at 750 °C for 4 h [13].

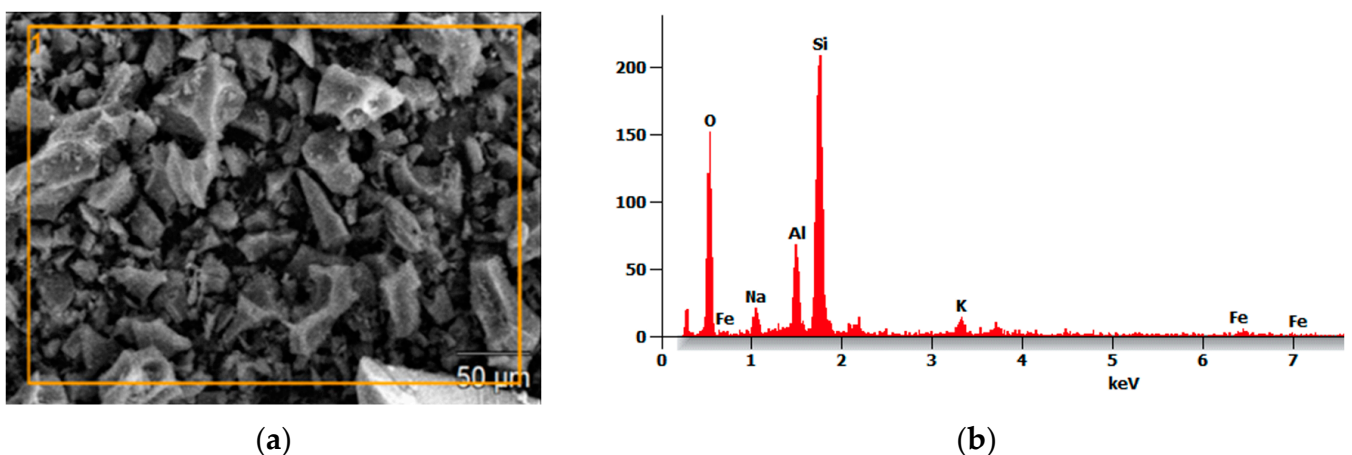


Figure 2. Microstructural analysis of PP: (a) Scanning Electron Micrograph and (b) EDS.

2.1.3. Metakaolin (MK)

MK was obtained through the calcination of PZ-400 kaolin in a furnace at 750 °C for 4 h. The main composition of this material is quartz and alumina, as shown in Figure 3b.

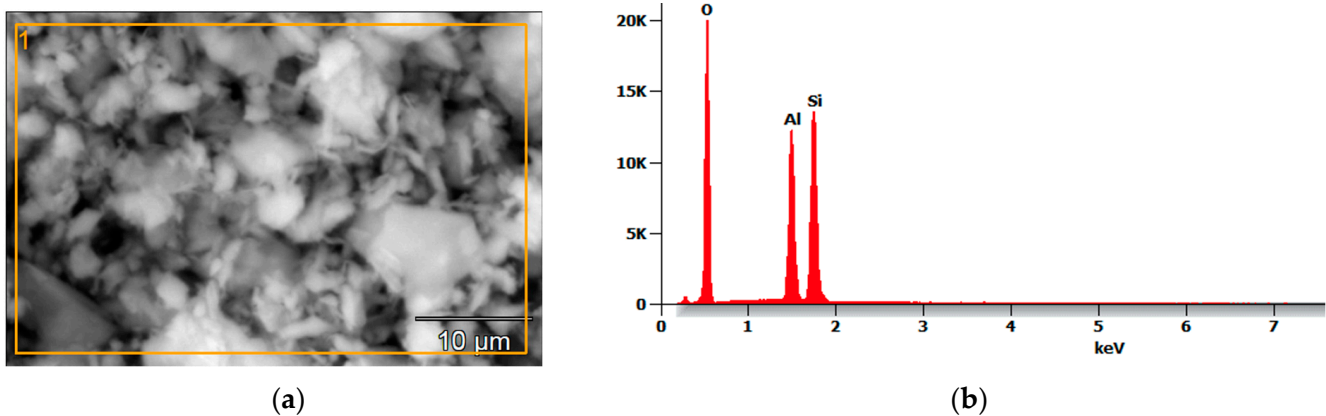


Figure 3. Microstructural analysis of MK: (a) Scanning Electron Micrograph; (b) EDS.

2.2. Methods

MTs and other raw materials were previously characterized in terms of their chemical composition, toxicology, and microstructure, as described in the materials section.

2.2.1. Preparation of Alkaline Activating Solution

Alkali-activator solution was prepared using commercial NaOH pellets and commercial sodium silicate solution (Na_2SiO_3) with a molar ratio ($\text{SiO}_2/\text{Na}_2\text{O}$) of 2.5. The activator solution was prepared 24 h before use to ensure complete activation of the reagents. NaOH granules were used to prepare a solution with a concentration of 10 M [21–24], while the prepared sodium silicate had a density of 1.53 g/cm^3 at $20 \text{ }^\circ\text{C}$ and a viscosity of 1.283 g/cm.s at the same temperature, with a total solids content of 45.26%. No flash setting was observed for sodium silicate to sodium hydroxide with a mixing ratio of 2.5, consistent with the observations of Rihan et al. [21].

2.2.2. Preparation of Geopolymer

MTs, previously characterized in terms of their chemical composition, toxicology, and microstructure, underwent a mechanochemical stabilization process before the geopolymerization step. The stabilization involved grinding the tailings with sodium sulfide nonahydrate ($\text{Na}_2\text{S}\cdot 9\text{H}_2\text{O}$) and elemental sulfur at 1% and 0.5% by weight, respectively, for 30 min in a ball mill at 60 rpm. The objective was to stabilize the metal cations and reduce the particle size of the tailings to less than $65 \text{ }\mu\text{m}$ (i.e., $d_{90} = 65 \text{ }\mu\text{m}$).

A full factorial design with three central points was previously used using Statgraphics Centurion 19-X64 software to evaluate the binder/mine tailings ratio (25/75, 45/55, 35/65), with compressive strength results obtained at 14 days, ranging between 28.31 and 46.34 MPa. The mathematical model explained 91.32% of the variability in compressive strength with a p value < 0.05 , recommending a binder/mine tailings ratio of 25/75, a curing temperature of $20 \text{ }^\circ\text{C}$, and a $\text{Na}_2\text{SiO}_3/\text{KOH}$ ratio of 3.5 for maximum strength.

In this context, MT mixes were prepared by mixing with 1% by weight of plasticizer in a planetary mixer at 160 rpm for 5 min. Then, MK and PP were added according to the formulation in Table 4 and mixed at 60 rpm for 5 min to homogenize the mixture.

Finally, the alkali-activator solution was added, with a volumetric ratio ($\text{NaOH}/\text{Na}_2\text{SiO}_3$) of 1.9. The mixture was stirred for 5 min at 60 rpm, followed by 10 min at 160 rpm until a paste-like and homogeneous aluminosilicate gel was obtained. This paste mixture was poured into 50 mm cubic molds and manually agitated to remove air bubbles.

The molds were sealed with adhesive tape and cured at $40 \text{ }^\circ\text{C}$ for 20 h or under ambient conditions ($20 \pm 2 \text{ }^\circ\text{C}$) for the same period. After curing, the specimens were demolded and transferred to a curing chamber with 80% relative humidity until compression strength tests at 7, 14, 28, and 56 days, as seen in Figure 4.

Table 4. Geopolymer formulation and alkaline activator solution.

Geopolymer	Bs * (%)	MT (%)	MT (gr)	Bs (gr)		Bs + MT (gr)	AAS **			AAS/Bs
				MK	PP		NaOH (gr)	Na ₂ SiO ₃ (gr)	AAS (gr)	
A0	0	100	750	0	0	750	64.18	188.6	252.78	0
B10	10	90	675	37.5	37.5	750	64.18	188.6	252.78	3.37
C20	20	80	600	75	75	750	64.18	188.6	252.78	1.69
D30	30	70	525	112.5	112.5	750	64.18	188.6	252.78	1.12
E40	40	60	450	150	150	750	64.18	188.6	252.78	0.84
F50	50	50	375	187.5	187.5	750	64.18	188.6	252.78	0.67
MK-PP	0	0	0	375	375	750	64.18	188.6	252.78	0.34

*: Binders (MK + PP); **: alkali-activator solution.

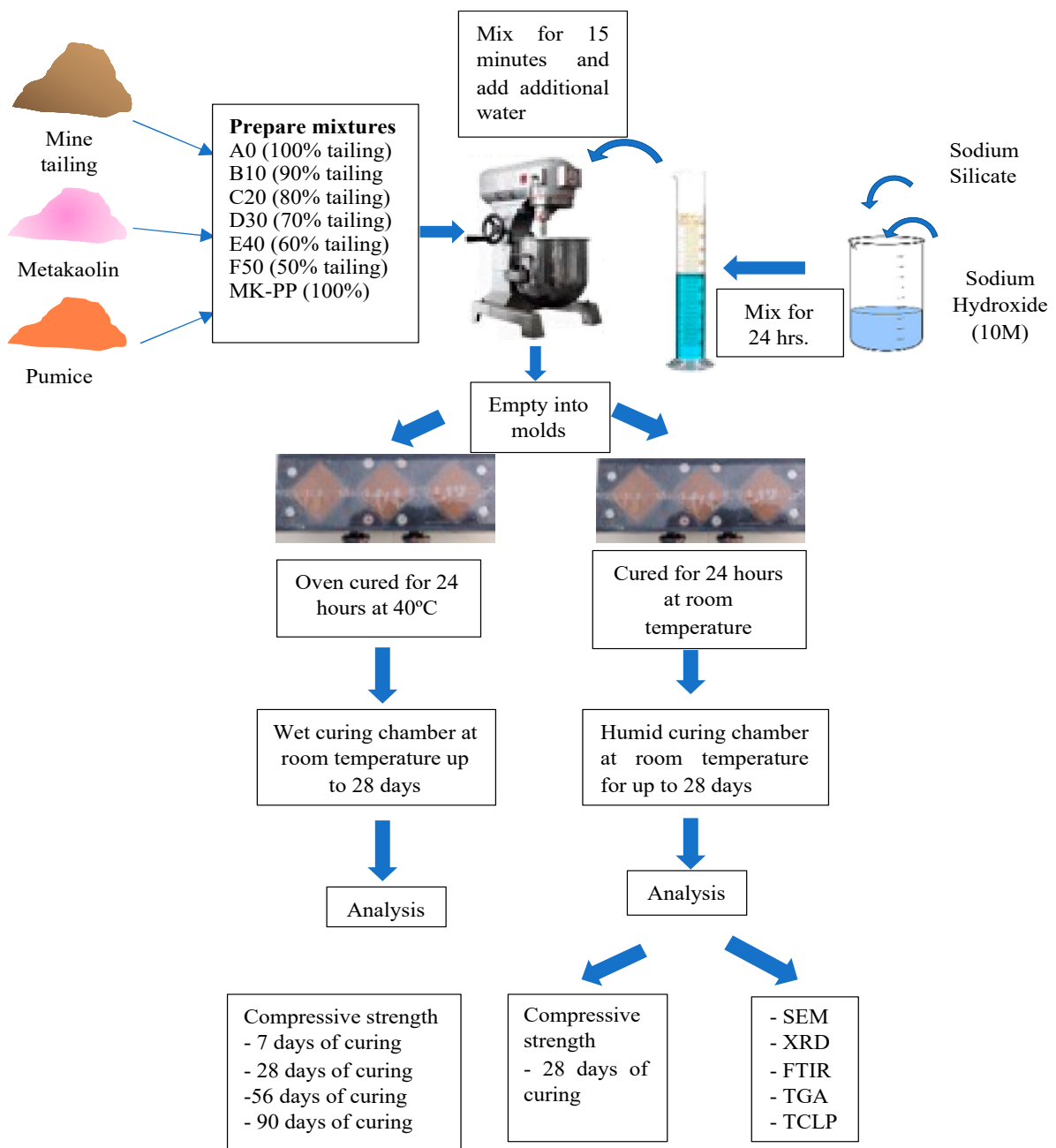


Figure 4. General process flow diagram for the production of mine tailings-based geopolymers.

2.3. Techniques for Characterization of Mine Tailings-Based Geopolymers

2.3.1. Mechanical Compression Strength

Tests were conducted following ASTM C-109 (Standard Test Method for Compressive Strength of Hydraulic Cement Mortars) using $50 \times 50 \times 50$ mm side cubic geopolymer specimens. A digital press ADR Touch 2000 from ELE International (Milton Keynes, UK) with a capacity of 2000 kN was employed. A constant load rate of 0.0609 cm per minute was used for the load application. Mechanical properties were evaluated using two approaches. The first set of geopolymers underwent initial curing at 40 °C for 20 h, while the second set cured at ambient temperature (20 ± 2 °C) for the same duration. Both sets were demolded and placed in a humid chamber (70% relative humidity) for scheduled monitoring. Evaluations for geopolymers cured at 40 °C were conducted at 7, 14, 28, 56, and 90 days, whereas geopolymers cured at ambient temperature (20 ± 2 °C) were evaluated only at 28 days.

Fragments resulting from the mechanical compression test of the block showing the best mechanical performance were used for microstructural and toxicological assays to assess microstructural stability and immobilization of the 5 PTHMs (As, Pb, Cd, Hg, and Zn).

2.3.2. Mineralogical Analysis of Geopolymers

X-ray diffraction (XRD) was used to characterize the mineral components of the MTs. A D8 Advance Diffractometer with Co Tube (38 kV, 25 mA) and wavelengths of $K\alpha_1$ equal to 1.78897 Å and $K\alpha_2$ equal to 1.79285 Å was used. It includes a Kbeta filter and a LynxEye XE detector with a measurement range of 2θ from 4° to 70°. Additionally, it is equipped with a database-driven phase identification using the International Centre for Diffraction Data (ICDD) PDF-2-2014, with quantification based on the Rietveld refinement method (TOPAS Structure Database).

2.3.3. Infrared Spectroscopic Analysis of Geopolymers

A PerkinElmer Frontier spectrometer (Waltham, MA, USA) was used, which performs two scans with a resolution of 4, using the MIR-TGS detector and a mid-range infrared source. This spectrometer has a scan speed of 0.2 cm/s and covers a range of 4000 to 400 cm^{-1} .

2.3.4. Morphological Analysis of Geopolymers

The samples are the same as those used for XRD and FTIR analyses. The equipment used was a THERMO SCIENTIFIC SCIOS 2 Scanning Electron Microscope (Waltham, MA, USA) to scan and examine the surface of the geopolymer, enabling measurement and evaluation of details.

2.3.5. Thermogravimetric Analysis

A PerkinElmer TGA 8000 thermogravimetric analyzer (Waltham, MA, USA) (TG/DTA, up to 1000 °C) was used to determine water loss temperatures (free, adsorbed, and chemically bound water) and the thermal decomposition of minerals in the geopolymer samples. The samples were loaded into a platinum crucible and heated from 40 to 1000 °C at 10 °C/min in a pure nitrogen atmosphere at a flow rate of 200 mL/min.

2.3.6. Toxicological Analysis of Geopolymers

To evaluate the environmental impact, leaching tests were conducted using the Toxicity Characteristic Leaching Procedure (TCLP) 1311 from the U.S. EPA. The process began by weighing 5 g of sample with a particle size less than 9 mm, then adding 96.5 mL of distilled and deionized water to form a homogeneous mixture. This mixture was stirred for 5 min on a magnetic stirrer to ensure complete dispersion of the sample.

Next, the pH of the solution was measured using a HANNA pH meter. If the pH obtained was equal to or less than 5, extraction solution No. 1 was chosen. Otherwise, 3.5 mL of 1 N hydrochloric acid was added to the mixture and homogenized again.

Then, this solution was heated to 50 °C for 10 min and subsequently cooled to room temperature, followed by a new pH measurement. If the resulting pH was equal to or less than 5 after this process, extraction solution No. 1 was used; otherwise, extraction solution No. 2 was selected.

Regarding the preparation of the extraction solutions, the following specific procedures were carried out: For extraction solution No. 1, precisely 64.3 mL of 1N NaOH was measured and diluted with distilled water to a total volume of 1 L of solution, ensuring that the resulting pH was within the range of 4.93 ± 0.05 . On the other hand, for extraction solution No. 2, exactly 5.7 mL of glacial acetic acid was measured in a flask and diluted with distilled water to a volume of 1 L of solution, ensuring that the final pH was within the range of 2.88 ± 0.05 .

Leaching of the selected sample: 5 g of material with a particle size less than 9.0 mm was weighed, maintaining a weight/volume ratio of 1/20. The sample was transferred to a suitable container and sealed tightly with tape to prevent possible leaks. It was then continuously stirred for a period of 18 ± 2 h at 20 ± 2 °C, followed by filtration using filter paper to obtain the leachate solution.

Subsequently, tests were conducted to determine the concentration of heavy metals present in the leachate, following the USEPA-SW-846 method "Test Methods for Evaluating Solid Waste". These analyses were performed using the ICP-OES technique with the PerkinElmer AVIO-550 max equipment at Analytics' Laboratories del Sur S.R.L.

3. Results

3.1. Mechanical Properties

Mechanical Compression Strength of Geopolymers with Initial Curing at 40 °C for 20 h

As shown in Figure 5, geopolymer A0, with a binder/MTs ratio of 0/100 (i.e., pure MTs as the solid precursor), exhibited a compressive strength of 6.27 MPa. With a 10% binder (i.e., binder/MTs ratio of 10/90), the strength increased by 27% compared to the initial value. Increasing the ratio to 20/80 improved the compressive strength by 109%, and at 30/70, the improvement rose to 185% compared to the initial value. However, increasing the binder/MTs ratio to 40/60 resulted in an 11% decrease; finally, with a ratio of 50/50, there was a slight increase of 2.4% compared to geopolymer E40. This behavior was consistent across all four evaluated periods.

It is understood that as the binder content increases, there is a general improvement in mechanical behavior at each evaluated period. This behavior is related to the increased content of reactive aluminosilicate binder materials, resulting in increased Si and Al, which are fundamental components for the formation of sodium aluminosilicate hydrate gels (Na-A-S-H).

At 7 days of curing, geopolymer D30 exhibited the best mechanical performance, followed by E40 and F50. By day 14, geopolymer F50 showed the best performance, followed by E40 and D30. At 28 and 56 days of curing, geopolymers F50 and E40 demonstrated the best mechanical results. In contrast, the MK-PP geopolymer, composed of 100% binder, achieved a maximum strength of 40.37 MPa at 56 days and a minimum of 22.95 MPa at 14 days, as shown in Figure 5. While the mean strength value shows a decline from 28 days to 56 days for some geopolymer types, the amount of change is insignificant as it falls within the strength variability range for each curing time. However, additional research is needed to evaluate the longer-term performance of such mixes.

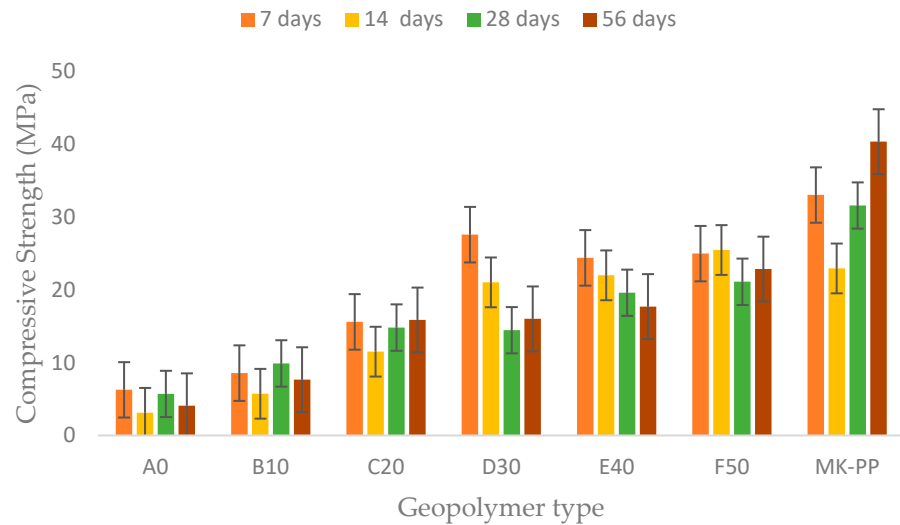


Figure 5. Mechanical behavior as a function of samples with different percentages of binder addition (MK-PP), ranging from 0% to 50%, and a 100% MK-PP specimen at 7, 14, 28, and 56 days of ambient temperature curing, and initial curing at 40 °C for 20 h.

Additionally, a significant portion of the compression strength is developed during the first week of curing, likely due to the initial thermal curing at 40 °C for 20 h. However, the trend towards decreasing mechanical behavior could be related to water loss during the thermal curing process.

Figure 6 presents the strength development for the two curing regimes at 28 days for the analyzed geopolymers. The data shown in blue pertain to specimens that underwent initial curing for 20 h at 40 °C in an oven, while the red line corresponds to initial curing for 20 h under ambient conditions (20 ± 2 °C). It is observed that geopolymers treated under ambient conditions during the first 20 h exhibit better performance.

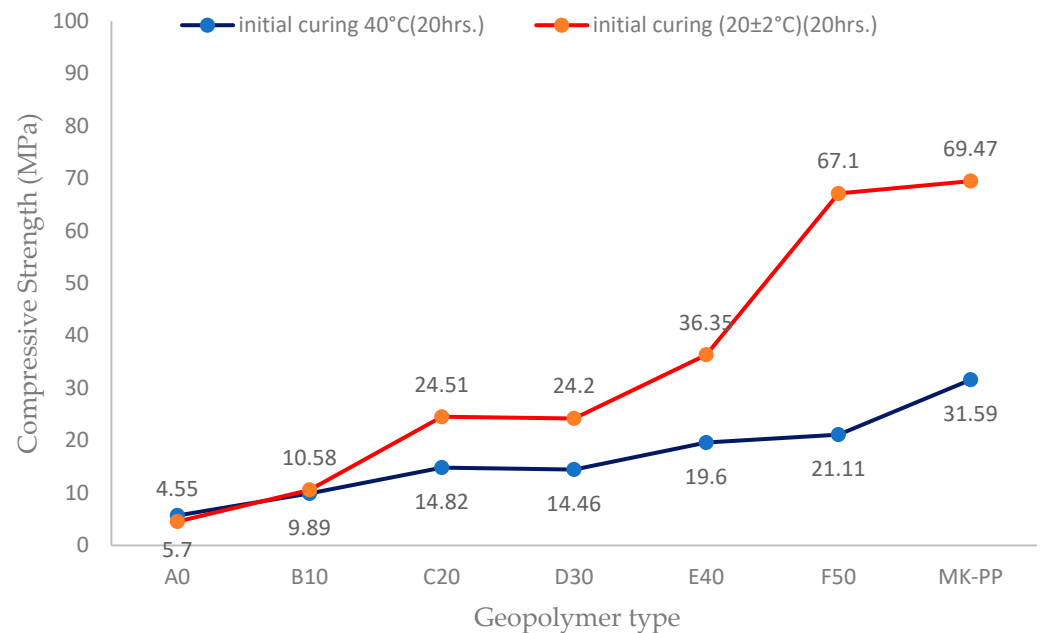


Figure 6. The 28-day compressive strength results for different geopolymer samples for two initial curing regimes.

For instance, at 28 days of curing, the geopolymer without binder reached a strength of 4.7 MPa, whereas the geopolymer with 50% binder achieved a maximum value of 67.1 MPa. In contrast, the geopolymer subjected to slightly elevated temperature curing during the

first 20 h at 40 °C shows nearly similar values, with a strength of 4.55 MPa without binder and a maximum of 21.11 MPa with 50% binder. Therefore, geopolymers treated under ambient conditions showed better mechanical development over time.

Figure 7 presents a comparison of compression strength results for two geopolymers cured under ambient conditions (one for 28 days and the other for 90 days). It is observed that geopolymer A0, cured for 90 days, experienced a 105% increase in compression strength compared to its counterpart, cured for 28 days.

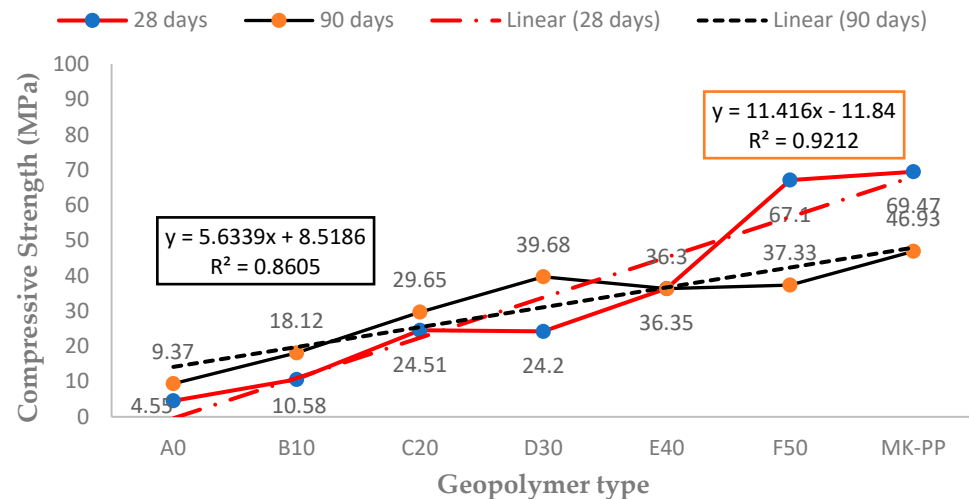


Figure 7. Comparative strength development of geopolymers at different curing times.

On the other hand, geopolymer D30 increases by 163%, while geopolymer E40 shows equal compression strength values at both 28 and 90 days. Additionally, geopolymer F50, cured for 28 days, exhibits better compression strength performance (an 80% increase) compared to its counterpart, cured for 90 days.

It can be deduced that curing time has a significant impact on mechanical properties. It is suggested that prolonging curing time may not be necessary, especially when using a higher percentage of MTs in geopolymer formation, with a 50/50 ratio achieving a compression strength of 67 MPa. This behavior follows a linear model with a correlation coefficient of 0.92, indicating a good fit for linear regression.

3.2. Mineralogical Analysis

XRD Analysis

Figure 8 presents the X-ray diffractogram of geopolymers with different amounts of binder. The A0 sample (100% MTs) shows the occurrence of sharp peaks, which suggests the formation of semi-crystalline to crystalline phases. The absence of a halo indicates that the geopolymeric material is not highly amorphous. Therefore, it is a geopolymer with low levels of geopolymerization due to the absence of aluminosilicate material from the binder. In the A0 geopolymer, the dominant phase is quartz, followed by pyrite and oligoclase. There is also a notable presence of calcium carbonate, likely due to exposure to CO₂ from the environment and the high calcium concentration in MTs.

In the other five samples, B10, C20, D30, E40, and F50, quartz was the dominant phase, with concentrations exceeding 60%. However, there was a decrease in the amount of quartz as the amount of binder in the geopolymer increased; from B10 to F50, the amount of quartz decreased from 67.4% to 61%. This pattern is also observed in pyrite, indicating that both phases were incorporated into the geopolymeric material, contributing to enhanced compression strength. Additionally, goethite showed a decrease from 5.2% to 1.9%, suggesting that both goethite and pyrite integrate into geopolymers in the form of Na (Fe)–A–S–H.

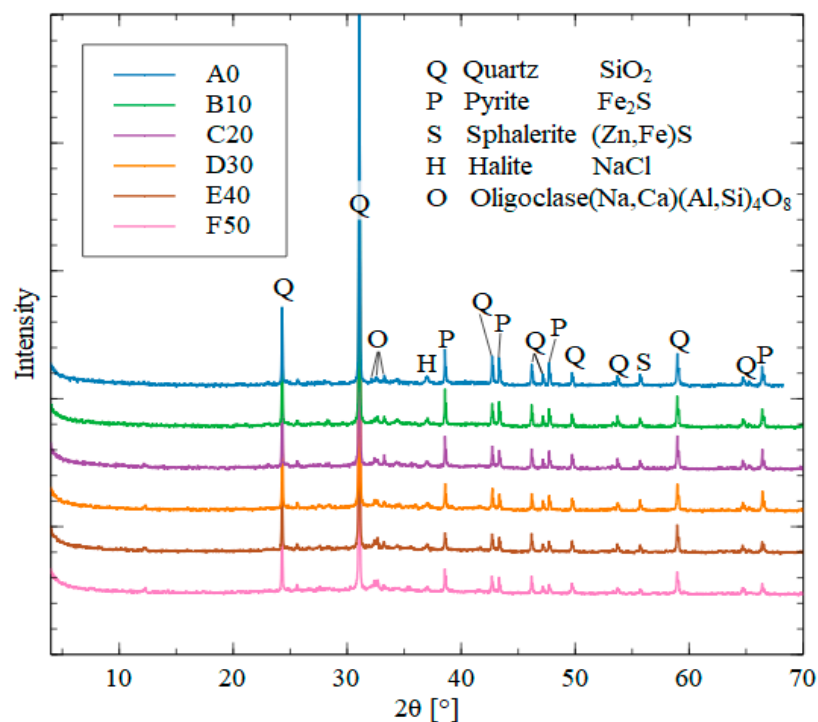


Figure 8. X-ray diffractogram of geopolymer samples A0, B10, C20, D30, E40 and F50.

In Figure 8, the diffractograms of samples D30, E40, and F50 show a halo between 20° and 40°, indicating the presence of amorphous material in the geopolymer. This is due to the predominance of aluminosilicate material from the binder. This behavior is characteristic of a geopolymeric material with good geopolymerization [25,26].

3.3. Infrared Spectroscopic Analysis of Geopolymer FTIR Analysis

FTIR Analysis

The FTIR spectrum, presented in Figure 9, showed that both the geopolymer and the raw materials consist primarily of Si–O and Al–O bonds due to the high content of aluminosilicates in the MTs and binder. Additionally, it was observed that H–O and H–O–H bonds could correspond to the presence of water molecules, while C–O bonds could be associated with the formation of alkaline carbonates due to environmental carbonation and the presence of calcite in the tailings. Figure 9 shows that the band located between 3250.48 and 3380 cm^{−1} corresponds to the stretching vibrations of the H–O bond of water molecules loosely bound to sodium aluminosilicate hydrate gels (N–A–S–H) [27]. Furthermore, the band around 1641 cm^{−1} is associated with the bending vibration of –OH from absorbed water [28].

The bands between 1448, 1452, and 1474 cm^{−1}, within the range of 1340 to 1460 cm^{−1}, correspond to the asymmetric stretching vibration of the C–O bond of CO₃^{2−} from Na₂CO₃, a compound formed by excess Na in geopolymers and atmospheric CO₂ [29], or from calcium carbonate formed due to the presence of calcium in MTs. The band near 1162 cm^{−1} is attributed to the asymmetric stretching vibration of the Si–O–Si bond and the bending vibration of the Al–O–Si bond, indicative of the presence of geopolymers and unreacted binder materials [28], present in all four analyzed samples.

Additionally, main bands are observed in all four samples in the range of 983 to 991 cm^{−1}, corresponding to the asymmetric stretching vibration of Si–O–T bonds (T = tetrahedral Si or Al). This indicates that the geopolymerization process has completed and stabilized due to the peak around 987–1010 cm^{−1} [30].

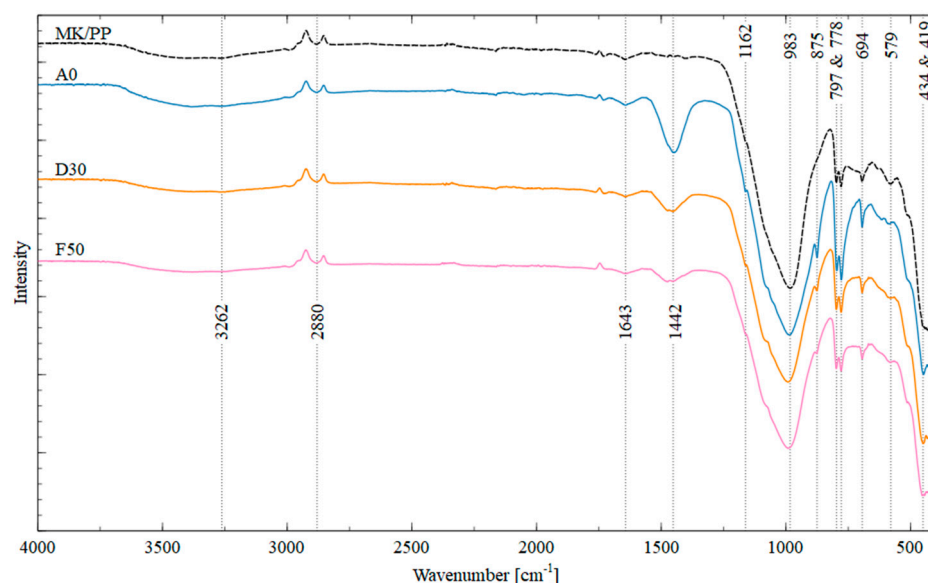


Figure 9. FTIR spectra of synthesized geopolymers: control geopolymer MK-PP, AO, D30, and F50.

On the other hand, the band present in three samples—except in the control sample at a wavelength of 875 cm^{-1} —is attributed to the stretching vibration of the Si–O bond and the bending vibration of OH from Si–OH groups.

The bands in the range of $797\text{ to }694\text{ cm}^{-1}$ are related to symmetric vibrations of Si–O–T bonds and appear in all four studied samples [28]. Finally, the bands between $450\text{ and }470\text{ cm}^{-1}$ correspond to the stretching vibrations of Si–O–Si and O–Si–O bonds [15,31], while the bands around 419 cm^{-1} present in all four studied samples are attributed to Fe^{2+}O^- vibrations [32].

3.4. Morphological Analysis of Geopolymers

SEM/EDS Analysis of Formed Geopolymers

Energy-dispersive X-ray spectroscopy (EDS) analysis was conducted on specific areas of the sample to obtain semi-quantitative data of Si, Al, Ca, Na, O, Mg, Cu, S, As, K, and Fe in different areas of the sample. The EDS spectra for geopolymers A0, B10, C20, D30, E40, F50, and MK-PP are shown in Figure 10, and the data are presented in Table 5.

Table 5. Comparative SEM/EDS analysis (% weight) in geopolymers samples.

Element	A0	B10	C20	D30	E40	F50	MK-PP
O	45.96	45.59	45.43	46.06	46.03	45.79	48.08
F	-	-	-	-	-	1.15	-
Na	5.53	4.90	5.64	6.06	6.41	5.84	6.41
Mg	0.85	0.69	-	0.85	0.75	0.65	0.56
Al	2.53	3.41	4.37	4.95	5.81	5.39	8.64
Si	24.11	23.51	24.38	23.91	25.37	24.96	31.99
S	5.15	4.63	3.83	4.41	3.04	3.47	-
Cl	1.17	0.86	1.13	0.88	0.71	0.53	-
K	0.84	0.99	0.98	1.03	1.15	0.80	1.20
Ca	2.12	2.70	2.35	2.15	1.81	1.64	0.97
Ti	-	0.18	-	-	0.13	0.12	-
Fe	10.10	11.52	10.29	8.91	7.51	8.32	1.45
Cu	0.97	-	-	-	-	-	0.66
As	0.93	1.03	10.29	0.80	1.28	1.33	0.03

The main contributors to good mechanical performance are the amorphous and semi-crystalline particles of MK and PP (made up of primarily Si and Al). From the EDS analysis,

it is evident that silicon is the most abundant element in all analyzed geopolymers, averaging 25%. The control geopolymer shows the highest percentage of silicon (32%), followed by Fe and Al, whose percentages increase from 2% to 8.64% in the control geopolymer, depending on the increase in binder material (MK and PP). Other important elements in the geopolymers include sodium and sulfur; the percentage of both decreases as the binder content increases (and MT content decreases).

It is noteworthy that one of the elements considered as heavy metals, As, appeared in the EDS analysis up to 10% in geopolymer C20, while in the other geopolymers, As was below 1%. Geopolymers contain a higher percentage of silicon, consistent with the FTIR spectra, where vibrations near a wavelength of 1162 cm^{-1} correspond to vibrations of Si–O–T bonds (T= rich in Si and Al), suggesting improved long-term mechanical compression resistance, provided they are cured under ambient conditions.

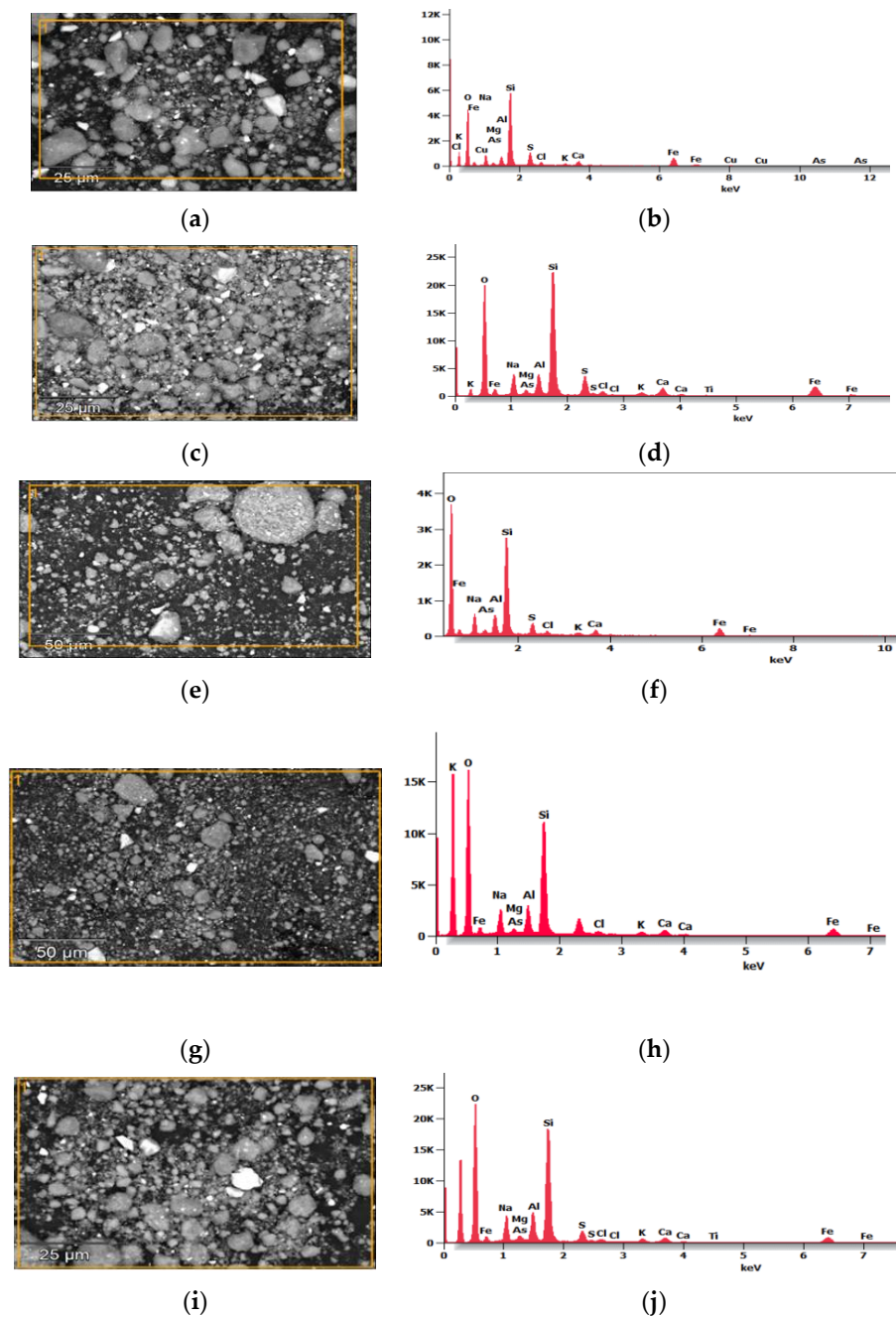


Figure 10. Cont.

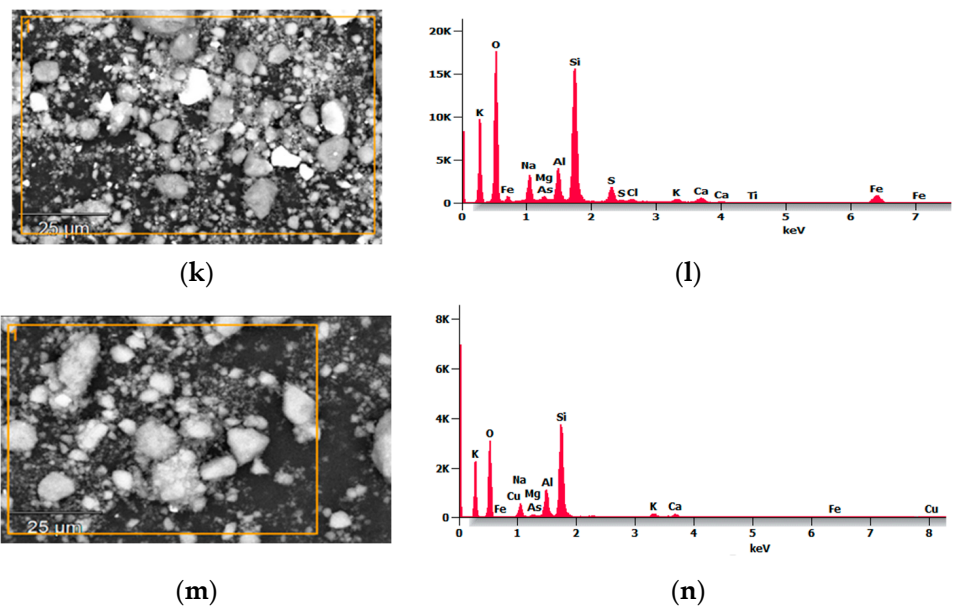


Figure 10. SEM/EDS images of geopolymers: (a,b): A0; (c,d): B10; (e,f): C20; (g,h): D30; (i,j): E40; (k,l): F50; and (m,n): MK-PP (powder state), respectively.

Figure 11 displays SEM microphotographs of the seven geopolymers. It can be observed that all of them exhibit microcracks, the quantity of which decreases as the binder material content in the geopolymers increases. Similarly, the average pore sizes are 7.47, 7.56, 7.48, 10.36, 5.43, 6.50, and 6.70 μm , indicating very similar microstructure among all the mix designs. Therefore, we could specify that the percentage variation of binder material is not associated with the variation in the pore size of the evaluated samples. Additionally, all geopolymers showed void volumes corresponding to air bubbles trapped during fabrication and subsequently expelled.

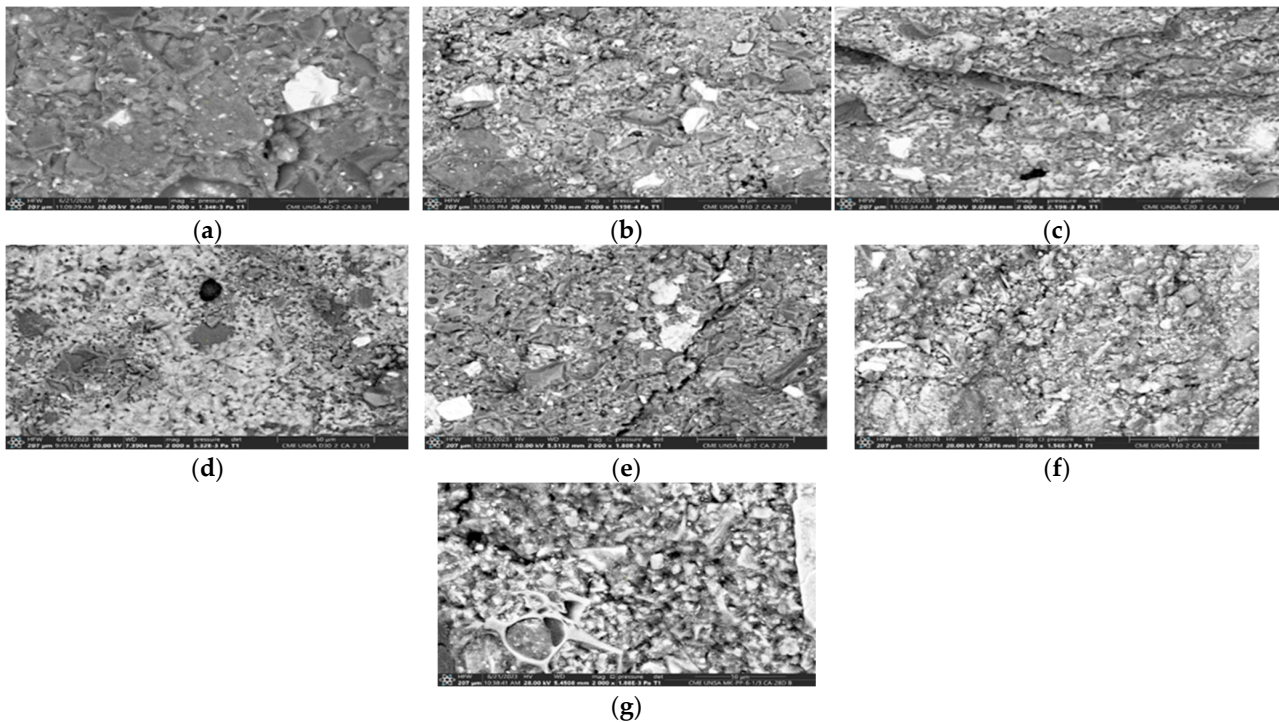


Figure 11. SEM images of geopolymers (a) A0, (b) B10, (c) C20, (d) D30, (e) E40, (f) F50, and (g) MK-PP (solid state).

The bulk density of geopolymers increases as the proportion of binder material increases. It is important to note that some unreacted source material remains even after the curing process is completed.

3.5. Thermogravimetric Analysis (TGA)

The mass loss of the sample (TGA) and the derivative weight (DTG) are shown in Figure 12a,b. The pozzolanic mixture-based control geopolymer (MK/PP) showed mass loss largely below 200 °C, which can be attributed to water evaporation within the sample. For the geopolymer samples, water evaporates in a similar temperature range but exhibits two distinct peaks in DTG. The first peak at 90 °C is caused by the evaporation of free water in the sample, while the second peak at 140 °C is attributed to the evaporation of water from capillary pores. Due to capillary tension in these voids, water evaporates at a temperature higher than its boiling point. The mass loss in this region (100 °C–220 °C) can also be attributed to water evaporation between layers, leading to dehydration of clay minerals.

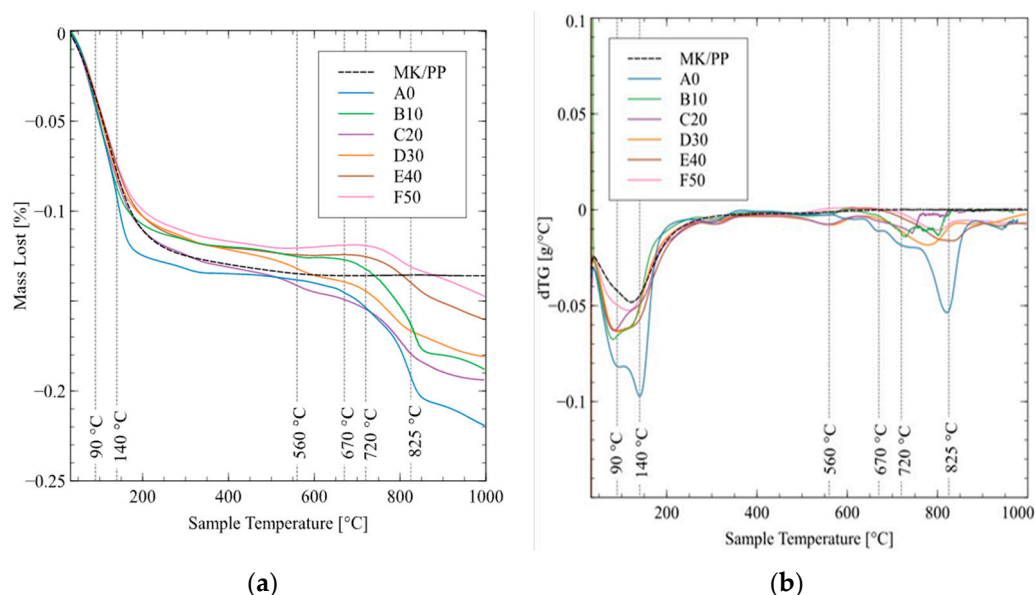


Figure 12. (a) Thermogravimetric and (b) differential thermogravimetric analysis of the geopolymers.

The mass loss peaks between 500 °C and 1000 °C are caused by the decomposition of various minerals found in the geopolymer samples. Between 400 °C and 450 °C, sulfides from iron sulfide minerals decompose, and between 400 °C and 480 °C, pyrite decomposes. Peaks at 670 °C and 720 °C can be attributed to the dihydroxylation of minerals in the parent rock, where terminal hydroxide groups (-OH) are removed during heating. Mass loss between 700 °C and 900 °C is caused by the decomposition of calcite in the sample, with a DTG peak at 825 °C.

On the other hand, in all samples, the greatest mass variation is observed between room temperature (20 ± 2 °C) and 200 °C. This mass loss is primarily attributed to the evaporation and loss of water inside the geopolymer structure. SEM analysis initially confirmed the presence of pores, and given that porosity is directly related to density, which in turn influences compressive strength, it can be inferred that this mass loss at 200 °C promotes the formation of structural defects such as pores and cracks [33]. Furthermore, it is important to note that the formation and reduction of pores are not solely due to water loss, as they can be influenced by other factors such as raw materials, the type of alkaline activator, and curing conditions.

3.6. Environmental Impact of Geopolymer

TCLP Analysis

In order to evaluate the efficiency of immobilizing metals and metalloids and to determine the environmental and hazardous waste impacts, a comparative study was conducted between the TCLP test (US EPA SW-846 method 1311), the Environmental Quality Standards (ECA) of Peru (Supreme Decree No. 011-2017-MINAM), and the Australian Ministry of Environment (NSW EPA 2014). This analysis considered the concentrations of five heavy metals and metalloids, detailed in Table 6, as well as the values of leachate concentrations from the five samples analyzed, which are specified in Table 7.

Table 6. Total toxic heavy metal content in Paraíso MTs.

Mine Tailing	Concentration of Heavy Metals and Metalloids (mg/kg)				
	As	Cd	Pb	Zn	Hg
Paraíso	6000	32.54	2081.87	2309.00	35.00

Table 7. Concentration of toxic heavy metals in MTs leachate and geopolymers.

Heavy Metals	Concentration of Heavy Metals and Metalloids (mg/L)				
	As	Cd	Pb	Zn	Hg
Paraíso MTs	0.393	0.046	0.590	1.828	0.401
A0	10.460	0.0660	0.105	5.4060	<0.004
B10	2.602	0.0250	0.197	6.8870	<0.004
C20	0.625	0.0160	0.099	7.7940	<0.004
D30	0.277	0.0150	0.067	7.4240	<0.004
E40	0.223	<0.0004	<0.006	7.2670	<0.004

From the analysis regarding the hazard classification of MTs and synthesized geopolymer material (see Table 8), we can observe the following: based on the data for arsenic (As), both the MTs and geopolymer samples A0-2, B10-2, C20-2, D30-2, and E40-2 would be classified highly hazardous materials because the concentration values exceed the threshold of 2000 mg/kg (NSW EPA 2014). In contrast, the metal cadmium (Cd) exhibits environmentally favorable results because its concentration values in both the material and leachates are below established thresholds, indicating effective geopolymerization processes for this element in particular.

Table 8. Hazardousness of synthesized geopolymers based on total metal concentrations in MTs and leachates.

Sample	Arsenic		Cadmium		Mercury		Lead		Zinc		Classification
	Conc. (mg/Kg)	TCLP (mL/L)	Conc. (mg/Kg)	TCLP (mL/L)	Conc. (mg/Kg)	TCLP (mL/L)	Conc. (mg/Kg)	TCLP (mL/L)	Conc. (mg/Kg)	TCLP (mL/L)	
MTs-P	6000	0.393	32.54	0.046	35	0.401	2081.87	0.59	2309	1.828	very hazardous material
A0	6000	10.460	32.54	0.0660	35	<0.004	2081.87	0.105	2309	5.4060	
B10	5400	2.602	29.25	0.0250	31.5	<0.004	1873.68	0.197	2078.1	6.8870	hazardous material
C20	4800	0.625	26.00	0.0160	28.00	<0.004	1665.49	0.099	1847.2	7.7940	
D30	4200	0.277	22.75	0.0150	24.5	<0.004	1457.31	0.067	1616.3	7.4240	No hazardous material
E40	3600	0.223	19.5	<0.0004	21.0	<0.004	1249.12	<0.006	1385.4	7.2670	

On the other hand, the heavy metal mercury (Hg) designates the MTs as hazardous material, while in the leachate from geopolymers, the concentrations are lower than the established limits. This indicates that geopolymerization was effective for the stabilization and solidification of mercury in the Paraíso mine tailings. However, lead appears with values above the thresholds in both MTs and geopolymers A0, B10, and C20, classifying them as environmentally hazardous materials. In contrast, geopolymers D30 and E40 are

classified as non-hazardous materials, which indicates that the higher amount of binder in those samples helped effectively immobilize the lead in the MTs.

For zinc, there is insufficient information to evaluate its hazard classification. Therefore, to prevent them from being considered potentially contaminating materials, all geopolymeric materials should have a minimum binder content in their mix design exceeding 30%.

The efficiency of heavy metal immobilization is primarily defined by strength and leaching resistance [34]. While strength development is considered an indicator of solidification, leaching tests are likely the most critical measure for assessing the stabilization degree of heavy metals [35]. Table 9 presents the consolidated immobilization efficiency results, expressed as percentages, for the toxic metals measured: arsenic, cadmium, lead, and mercury, across different geopolymer formulations.

The literature [36] indicates that geopolymers are inorganic polymers with excellent properties suitable for the stabilization/solidification of hazardous contaminants. According to them, stabilization/solidification mechanisms for cationic heavy metals include physical encapsulation, adsorption, precipitation, and binding within a silicate structure. However, they note that geopolymers have poor performance in immobilizing anions due to repulsion effects, which leads to high leaching. Despite this, they argue that through electrostatic interactions, it is possible to trap metalloids such as arsenic and selenium present in MTs.

Figure 13 shows the efficiency of immobilization of selected metals and metalloids. Geopolymers showed low efficiency in the immobilization of anions unless the mix design contained at least 30%–40% binder material, where a maximum immobilization efficiency of 40% is achieved. In contrast, geopolymers showed better immobilization efficiency for metals. Cadmium exhibits an immobilization range between 45% and 99% with 40% binder content, while lead achieves an immobilization of 70% to 99%. Mercury, on the other hand, reaches up to 99% immobilization, even in geopolymers composed solely of MT-type materials. These results indicate effective metal immobilization, in contrast to the metalloid arsenic, which does not achieve the same level of efficiency. No immobilization of As is observed in formulations A0, B10, and C20, nor of Cd in A0. These differences in immobilization are likely associated with the presence and proportion of binders in the specimen composition.

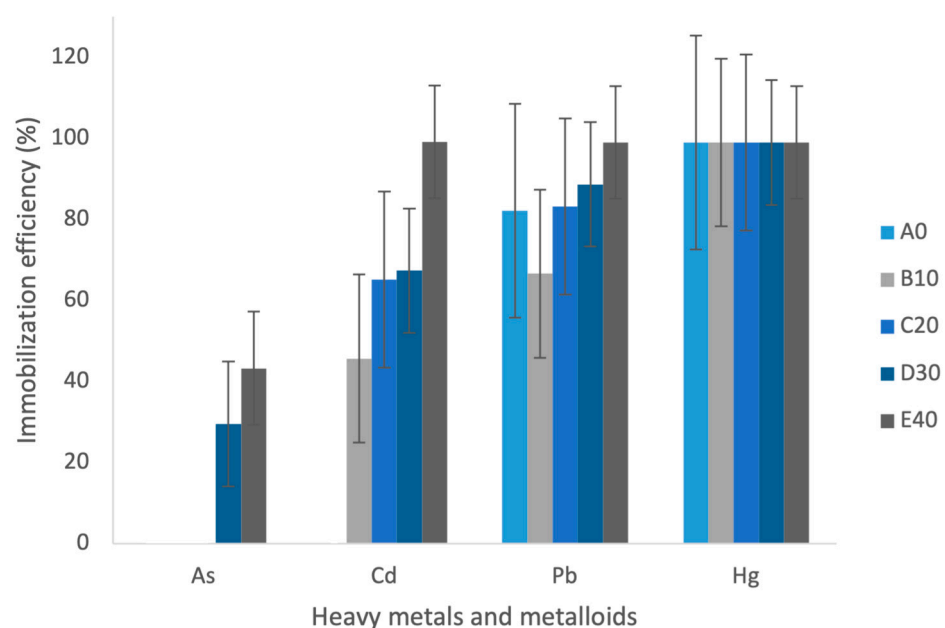


Figure 13. Efficiency of heavy metal immobilization process.

Table 9. The concentration of toxic heavy metals in MTs leachate and geopolymers.

Geopolymer	Toxic Heavy Metal Immobilization Efficiency (%)			
	As	Cd	Pb	Hg
A0	0.00	0.00	82.20	99.00
B10	0.00	45.65	66.61	99.00
C20	0.00	65.22	83.22	99.00
D30	29.52	67.39	88.64	99.00
E40	43.26	99.13	98.98	99.00

4. Discussion

The mechanical strength values of the samples matched or exceeded those obtained by Wan [15]. The observed behavior of strength increasing with higher binder content but decreasing when reaching a 40/60 ratio is consistent with other studies [8,15].

Similarly, the results of this study align with findings reported by Elnour [37], who observed that the incorporation of ground granulated blast-furnace slag (GGBFS) reduced porosity and microcracks in geopolymeric samples, resulting in a denser and more compact microstructure. This led to a greater amount of geopolymer gel, which efficiently coated the particle surfaces, enhancing matrix cohesion and compressive strength.

The molarity of NaOH (M) and the binder/liquid ratio (AL/B) have a more significant influence on compressive strength than the sodium silicate/sodium hydroxide ratio (SS/SH), as observed in Nithin's study [38].

The work presented by Wang [39] demonstrated the efficient use of lead and zinc tailings with low silicon and aluminum content to produce geopolymer with remarkable mechanical and immobilizing properties. The geopolymer achieved a compressive strength of 52.8 MPa at 28 days. The optimization of raw material compositions significantly impacted its performance. A higher slag content favored polymerization and improved gel structure, while an increase in metakaolin intensified zeolite formation but also generated low-polymerization NASH gels with poor bonding properties, leading to microcracks and heterogeneity.

Research conducted by Burciaga-Diaz [40] and Rovnaník [41] demonstrated that curing geopolymers at temperatures above 60 °C promoted rapid early-age compressive strength gain. However, curing at 20 °C ± 2 °C (ambient temperature) is more effective in the long term, promoting greater progress in reaction processes, resulting in denser microstructures with high compressive strength. Geopolymers cured under ambient conditions show better mechanical development over time, suggesting greater formation of sodium–aluminum silicate hydrate (N–A–S–H) gels, consistent with Paiva's findings [42].

The immobilization of arsenic (As) was greater than 30% after the substitution of 30% or more of binder (D30-E40) in the mixture design, suggesting that the efficiency in the immobilization of As is related to a greater presence of binders. In contrast, cadmium (Cd) and lead (Pb) were 99% immobilized from a 40% binder substitution (E40). On the other hand, mercury (Hg) was immobilized even in the absence of binders, which indicated that the immobilization of this metal could be associated with both the previous stabilization and the solidification process of the MTs using geopolymerization technology. These results are consistent with the findings of Karoui et al. [43], who used the reactive geopolymerization method for inertization. The low immobilization of As is attributed to the fact that by forming oxyanions, elements such as As, Sb, V, and B have greater leachability in the alkaline conditions of the geopolymer gel.

5. Conclusions

The main conclusions of this experimental study are summarized as follows:

- This study showed that the highest compressive strength of the geopolymer based on MTs, MK, and PP was achieved under specific conditions, including a concentration of 10 M NaOH, a Na₂SiO₃/NaOH ratio of 1.9, and a curing temperature of 20 ± 2 °C.

Using 50% MTs and 50% binder (MK and PP) ratio, the geopolymer achieved a compressive strength of 67 MPa at 28 days of curing.

- Mechanical properties were influenced by curing time, especially when higher percentages of MT were used and prolonged curing was not necessary. The high compressive strength values could be explained by SEM/EDS analyses, where quartz and pyrite phases initially decreased significantly, indicating their incorporation into the geopolymer. Specimens demonstrated microstructural stability with an average pore size of 7.21 μm .
- Curing time influenced the gain in compressive strength. For example, specimen F50, compared to specimen A0, experienced a 300%, 270%, and 461% increase in strength at 7, 28, and 56 days of curing. However, prolonging the curing time with MT percentages equal to or greater than 50% is not recommended, based on previous studies on the interaction between curing temperature and the binder/mining tailings ratio.
- The geopolymerization process effectively immobilized heavy metals; however, arsenic was present in higher-than-expected quantities, indicating the need for further research to improve arsenic immobilization in the process.
- Additionally, geopolymers with 30% and 40% binder replacement showed better performance in immobilizing heavy metals, classifying them as non-hazardous materials since contaminant concentrations did not exceed the standards set by NSW EPA 2014. However, if the geopolymer contains less than 30% replacement, some heavy metals, such as lead (Pb) or mercury (Hg), may exceed these limits.
- The addition of binders such as MK and PP not only improved the mechanical properties of the geopolymer but also promoted the stabilization and encapsulation of MTs, thereby contributing to the production of safer and higher-performance materials.

Author Contributions: Conceptualization, G.P. and H.B.; methodology, G.P.; software, G.P. and C.C.; data validation, G.P. and A.H.; formal analysis, A.H. and C.C.; research, G.P.; resources, H.B. and R.H.; data curation, G.P.; writing: preparing the original draft G.P.; writing: review and editing, A.H., C.C., H.B., and R.H.; visualization, G.P.; supervision, G.P. and H.B.; project management, G.P.; acquisition of financing, H.B. and R.H. All authors have read and agreed to the published version of the manuscript.

Funding: This research was funded by the Universidad Nacional de San Agustín de Arequipa—Perú, according to the financing contract number IBAIB-10-2019-UNSA, competition “Investigación básica aplicada en ingeniería, ciencias y biomédicas”, call 2018-2 B.

Data Availability Statement: The original contributions presented in the study are included in the article, further inquiries can be directed to the corresponding author.

Acknowledgments: The authors gratefully acknowledge the financial assistance provided by the Universidad Nacional de San Agustín de Arequipa—Perú to carry out this research [contract numbers: IBAIB-10-2019-UNSA]. As well as Oscar Jesús Flores Avendaño, Lic Miguel Ángel Alarcón García, and Andrea Del Pilar Machaca Arcana for their valuable support in the administrative and logistical aspects.

Conflicts of Interest: The authors declare that there are no conflicts of interest. In addition, the sponsors had no role in the design, execution, interpretation or writing of the study.

References

1. Taghipour, M.; Jalali, M. Heavy Metal Release from Some Industrial Wastes: Influence of Organic and Inorganic Acids, Clay Minerals, and Nanoparticles. *Pedosphere* **2018**, *28*, 70–83. [[CrossRef](#)]
2. González-Valoys, A.C.; Arrocha, J.; Monteza-Destro, T.; Vargas-Lombardo, M.; Esbrí, J.M.; Garcia-Ordiales, E.; Jiménez-Ballesta, R.; García-Navarro, F.J.; Higuera, P. Environmental Challenges Related to Cyanidation in Central American Gold Mining; the Remance Mine (Panama). *J. Env. Manag.* **2022**, *302*, 113979. [[CrossRef](#)] [[PubMed](#)]
3. Saeed, A.; Najm, H.M.; Hassan, A.; Sabri, M.M.S.; Qaidi, S.; Mashaan, N.S.; Ansari, K. Properties and Applications of Geopolymer Composites: A Review Study of Mechanical and Microstructural Properties. *Materials* **2022**, *15*, 8250. [[CrossRef](#)] [[PubMed](#)]
4. Ji, Z.; Pei, Y. Bibliographic and Visualized Analysis of Geopolymer Research and Its Application in Heavy Metal Immobilization: A Review. *J. Environ. Manag.* **2019**, *231*, 256–267. [[CrossRef](#)]
5. Tian, Q.; Bai, Y.; Pan, Y.; Chen, C.; Yao, S.; Sasaki, K.; Zhang, H. Application of Geopolymer in Stabilization/Solidification of Hazardous Pollutants: A Review. *Molecules* **2022**, *27*, 4570. [[CrossRef](#)]

6. Davidovits, J. Geopolymers: Ceramic-like Inorganic Polymers. *J. Ceram. Sci. Technol.* **2017**, *8*, 335–350. [[CrossRef](#)]
7. Sikder, A.; Mishra, J.; Nanda, B.; Patro, S.K. Geopolymer Concrete as a Revolutionary Green Building Material for Modern Infrastructures. In *Encyclopedia of Green Materials*; Springer Nature: Singapore, 2022; pp. 1–9. [[CrossRef](#)]
8. Wan, Q.; Rao, F.; Song, S.; García, R.E.; Estrella, R.M.; Patiño, C.L.; Zhang, Y. Geopolymerization Reaction, Microstructure and Simulation of Metakaolin-Based Geopolymers at Extended Si/Al Ratios. *Cem. Concr. Compos.* **2017**, *79*, 45–52. [[CrossRef](#)]
9. Lazorenko, G.; Kasprzhitskii, A.; Shaikh, F.; Krishna, R.S.; Mishra, J. Utilization Potential of Mine Tailings in Geopolymers: Physicochemical and Environmental Aspects. *Process Saf. Environ. Prot. Inst. Chem. Eng.* **2021**, *147*, 559–577. [[CrossRef](#)]
10. Xiaolong, Z.; Shiyu, Z.; Hui, L.; Yingliang, Z. Disposal of Mine Tailings via Geopolymerization. *J. Clean. Prod.* **2021**, *284*, 124756. [[CrossRef](#)]
11. Youssf, O.; Mills, J.E.; Elchalakani, M.; Alanazi, F.; Yosri, A.M. Geopolymer Concrete with Lightweight Fine Aggregate: Material Performance and Structural Application. *Polymers* **2022**, *15*, 171. [[CrossRef](#)]
12. Elemam, W.E.; Tahwia, A.M.; Abdellatif, M.; Youssf, O.; Kandil, M.A. Durability, Microstructure, and Optimization of High-Strength Geopolymer Concrete Incorporating Construction and Demolition Waste. *Sustainability* **2023**, *15*, 15832. [[CrossRef](#)]
13. Khattab, S.A.; Elshikh, M.M.Y.; Elemam, W.E.; Elshami, A.A.; Youssf, O. Effect of Magnetized Water-Based Alkaline Activator on Geopolymer Concrete Mechanical Performance and Durability. *Sustainability* **2023**, *15*, 16315. [[CrossRef](#)]
14. Kiventerä, J.; Lancellotti, I.; Catauro, M.; Poggetto, F.D.; Leonelli, C.; Illikainen, M. Alkali Activation as New Option for Gold Mine Tailings Inertization. *J. Clean. Prod.* **2018**, *187*, 76–84. [[CrossRef](#)]
15. Wan, Q.; Rao, F.; Song, S.; Zhang, Y. Immobilization Forms of ZnO in the Solidification/Stabilization (S/S) of a Zinc Mine Tailing through Geopolymerization. *J. Mater. Res. Technol.* **2019**, *8*, 5728–5735. [[CrossRef](#)]
16. Almalkawi, A.T.; Hamadna, S.; Soroushian, P. One-Part Alkali Activated Cement Based Volcanic Pumice. *Constr. Build. Mater.* **2017**, *152*, 367–374. [[CrossRef](#)]
17. Yadollahi, M.M.; Benli, A.; Demirboga, R. The Effects of Silica Modulus and Aging on Compressive Strength of Pumice-Based Geopolymer Composites. *Constr. Build. Mater.* **2015**, *94*, 767–774. [[CrossRef](#)]
18. Qaidi, S.M.A.; Tayeh, B.A.; Zeyad, A.M.; de Azevedo, A.R.G.; Ahmed, H.U.; Emad, W. Recycling of Mine Tailings for the Geopolymers Production: A Systematic Review. *Case Stud. Constr. Mater.* **2022**, *16*, e00933. [[CrossRef](#)]
19. Simonsen, A.M.T.; Solismaa, S.; Hansen, H.K.; Jensen, P.E. Evaluation of Mine Tailings' Potential as Supplementary Cementitious Materials Based on Chemical, Mineralogical and Physical Characteristics. *Waste Manag.* **2020**, *102*, 710–721. [[CrossRef](#)]
20. Felaous, K.; Aziz, A.; Achab, M.; Fernández-Raga, M.; Benzaouak, A. Optimizing Alkaline Activation of Natural Volcanic Pozzolan for Eco-Friendly Materials Production: An Investigation of NaOH Molarity and Na₂SiO₃-to-NaOH Ratio. *Sustainability* **2023**, *15*, 4453. [[CrossRef](#)]
21. Rihan, M.A.M.; Onchiri, R.O.; Gathimba, N.; Sabuni, B. Effect of elevated temperature on the mechanical properties of geopolymer concrete: A critical review. *Discov. Civ. Eng.* **2024**, *1*, 24. [[CrossRef](#)]
22. Phoo-ngernkham, T.; Maegawa, A.; Mishima, N.; Hatanaka, S.; Chindaprasirt, P. Effects of sodium hydroxide and sodium silicate solutions on compressive and shear bond strengths of FA-GBFS geopolymer. *Constr. Build. Mater.* **2015**, *1*, 1–8. [[CrossRef](#)]
23. Sunarsih, E.S.; As'ad, S.; Mohd Sam, A.R.; Kristiawan, S.A. The effect of sodium hydroxide molarity on setting time, workability, and compressive strength of fly ash-slag-based geopolymer mortar. *J. Phys. Conf. Ser.* **2023**, *2556*, 012019. [[CrossRef](#)]
24. Silva, M.C.D.; Racanelli, L.D.A.; Souza, J.A.D.S.; Quaresma, J.N.N.; Corrêa, M.S. Estudo do desempenho mecânico de geopolímero produzido com auto teor de ferro. *Matér Rio Jan.* **2023**, *28*, e20220309. [[CrossRef](#)]
25. Churata, R.; Almirón, J.; Vargas, M.; Tupayachy-Quispe, D.; Torres-Almirón, J.; Ortiz-Valdivia, Y.; Velasco, F. Study of Geopolymer Composites Based on Volcanic Ash, Fly Ash, Pozzolan, Metakaolin and Mining Tailing. *Buildings* **2022**, *12*, 1118. [[CrossRef](#)]
26. Sedira, N.; Castro-Gomes, J. Effect of Activators on Hybrid Alkaline Binder Based on Tungsten Mining Waste and Ground Granulated Blast Furnace Slag. *Constr. Build. Mater.* **2020**, *232*, 117176. [[CrossRef](#)]
27. Li, C.; Ouyang, J.; Yang, H. Novel Sensible Thermal Storage Material from Natural Minerals. *Phys. Chem. Miner.* **2013**, *40*, 681–689. [[CrossRef](#)]
28. Figueiredo, R.A.M.; Silveira, A.B.M.; Melo, E.L.P.; Costa, G.Q.G.; Brandão, P.R.G.; Aguilar, M.T.P.; Henriques, A.B.; Mazzinghy, D.B. Mechanical and Chemical Analysis of One-Part Geopolymers Synthesised with Iron Ore Tailings from Brazil. *J. Mater. Res. Technol.* **2021**, *14*, 2650–2657. [[CrossRef](#)]
29. Pan, Z.; Hu, S.; Zhang, C.; Zhou, T.; Hua, G.; Li, Y.; Lv, X. Mechanical and Hydration Characteristics of Stabilized Gold Mine Tailings Using a Sustainable Industrial Waste-Based Binder. *Materials* **2023**, *16*, 634. [[CrossRef](#)]
30. Longhi, M.A.; Rodríguez, E.D.; Bernal, S.A.; Provis, J.L.; Kirchheim, A.P. Valorisation of a Kaolin Mining Waste for the Production of Geopolymers. *J. Clean. Prod.* **2016**, *115*, 265–272. [[CrossRef](#)]
31. Catauro, M.; Papale, F.; Lamanna, G.; Bollino, F. Geopolymer/PEG Hybrid Materials Synthesis and Investigation of the Polymer Influence on Microstructure and Mechanical Behavior. *Mater. Res.* **2015**, *18*, 698–705. [[CrossRef](#)]
32. Ferreira, I.C.; Galéry, R.; Henriques, A.B.; Paula De Carvalho Teixeira, A.; Prates, C.D.; Lima, A.S.; Souza Filho, I.R. Reuse of Iron Ore Tailings for Production of Metakaolin-Based Geopolymers. *J. Mater. Res. Technol.* **2022**, *18*, 4194–4200. [[CrossRef](#)]
33. Burciaga-Díaz, O.; Escalante-García, J.I.; Magallanes-Rivera, R.X. Resistencia a La Compresión y Evolución Microestructural de Geopolímeros Base Metacaolín Expuestos a Alta Temperatura. *Rev. ALCONPAT* **2015**, *5*, 58–75. [[CrossRef](#)]
34. Malviya, R.; Chaudhary, R. Factors Affecting Hazardous Waste Solidification/Stabilization: A Review. *J. Hazard. Mater.* **2006**, *137*, 267–276. [[CrossRef](#)] [[PubMed](#)]

35. Vu, T.H.; Gowripalan, N. Mechanisms of Heavy Metal Immobilisation Using Geopolymerisation Techniques—A Review. *J. Adv. Concr. Technol. Jpn. Concr. Inst.* **2018**, *16*, 124–135. [[CrossRef](#)]
36. Tian, Q.; Guo, B.; Sasaki, K. Immobilization Mechanism of Se Oxyanions in Geopolymer: Effects of Alkaline Activators and Calcined Hydrotalcite Additive. *J. Hazard. Mater.* **2020**, *387*, 121994. [[CrossRef](#)]
37. Elnour Hamed, A.; Demiröz, A. Optimization of geotechnical characteristics of clayey soils using fly ash and granulated blast furnace slag-based geopolymer. *Constr Build Mater.* **2024**, *441*, 137488. [[CrossRef](#)]
38. Nithin, A.V.; Deepa Raj, S.; Soman, M. Optimizing the compressive strength of low-grade hydrous clay and copper slag-based sustainable ternary blended geopolymer mortar. *J Build Eng.* **2024**, *90*, 109431. [[CrossRef](#)]
39. Wang, H.; Wang, L.; Ren, Z.; Liu, S. Optimizing raw material composition and alkali content in low silicon-aluminum tailings-based geopolymers. *Constr Build Mater.* **2023**, *404*, 133339. [[CrossRef](#)]
40. Burciaga-Diaz, O.; Escalante-Garcia, J.I.; Gorokhovskiy, A. Geopolymers Based on a Coarse Low-Purity Kaolin Mineral: Mechanical Strength as a Function of the Chemical Composition and Temperature. *Cem. Concr. Compos.* **2012**, *34*, 18–24. [[CrossRef](#)]
41. Rovnaník, P. Effect of Curing Temperature on the Development of Hard Structure of Metakaolin-Based Geopolymer. *Constr Build Mater* **2010**, *24*, 1176–1183. [[CrossRef](#)]
42. Paiva, H.; Yliniemi, J.; Illikainen, M.; Rocha, F.; Ferreira, V.M. Mine Tailings Geopolymers as Awaste Management Solution for a More Sustainable Habitat. *Sustainability* **2019**, *11*, 995. [[CrossRef](#)]
43. Karoui, O.; Andrejkovičová, S.; Pato, P.; Patinha, C.; Perná, I.; Římnáčková, D.; Hajjaji, W.; Ascensão, G.; Rocha, F.; Mlayah, A. Alkali-activated geopolymers based on calcined phosphate sludges and metakaolin. *Environ. Sci. Pollut. Res.* **2024**, *31*, 45138–45161. [[CrossRef](#)] [[PubMed](#)]

Disclaimer/Publisher’s Note: The statements, opinions and data contained in all publications are solely those of the individual author(s) and contributor(s) and not of MDPI and/or the editor(s). MDPI and/or the editor(s) disclaim responsibility for any injury to people or property resulting from any ideas, methods, instructions or products referred to in the content.